Invisible Image Watermarks Are Provably Removable Using Generative AI

Xuandong Zhao[†*], Kexun Zhang[†*], Zihao Su[†], Saastha Vasan[†], Ilya Grishchenko[†],
Christopher Kruegel[†], Giovanni Vigna[†], Yu-Xiang Wang[†], Lei Li[‡]
[†]University of California, Santa Barbara, [‡]Carnegie Mellon University
[*]Equal contribution

Abstract—Invisible watermarks safeguard images' copyright by embedding hidden messages only detectable by owners. They also prevent people from misusing images, especially those generated by AI models. We propose a family of regeneration attacks to remove these invisible watermarks. The proposed attack method first adds random noise to an image to destroy the watermark and then reconstructs the image. This approach is flexible and can be instantiated with many existing image-denoising algorithms and pre-trained generative models such as diffusion models. Through formal proofs and empirical results, we show that all invisible watermarks are vulnerable to the proposed attack. For a particularly resilient watermark, RivaGAN, regeneration attacks remove 93-99% of the invisible watermarks while the baseline attacks remove no more than 3%. However, if we do not require the watermarked image to look the same as the original one, watermarks that keep the image semantically similar can be an alternative defense against our attack. Our finding underscores the need for a shift in research/industry emphasis from invisible watermarks to semantically similar ones. Code is available at https://github.com/XuandongZhao/WatermarkAttacker.

1. Introduction

Invisible watermarks on digital images have long been used in protecting the content of the image from misuse [1, 2, 3]. They do so by embedding hidden messages in images that can later be identified by a detection algorithm and used as evidence for various purposes. Their broad applications include transaction tracking [4], proof of ownership [5], copy control [6], authentication [7] and many others [8].

The era of generative AI has seen a new and more challenging application of invisible watermarks - telling images that are generated by an AI model from human-created ones. This application is particularly important and difficult because visual differences between AI-generated images and real images are becoming hard to identify as AI models get stronger, making watermarks one of the few methods that still work for AI-generation identification. Generative models such as DALL-E [9], Imagen [10] and Stable Diffusion [11] are able to produce both photo-realistic and artistic images that are often visually indistinguishable from the works of human photographers and artists. Such visual indistinguishability may lead to false beliefs in the

Figure 1: AI-generated fake images from Twitter depicting the arrest of Donald Trump.

content of the image and create misunderstandings (see examples in Figure 1).

To address these challenges, major AI companies such as Google [12], Microsoft [13], Meta [14], and OpenAI [15] have pledged to add *watermarks* to the content generated by their AI products, as government leaders [16] and legislators [17] start working on promoting and regulating responsible and ethical use of AI. *Invisible* watermarks are preferred because it preserves the image quality and it is less likely for a layperson to tamper with it. On the other hand, abusers are not laypersons. They are well aware of the watermark being added and will make a deliberate attempt to remove these watermarks. Therefore, it is crucial that the injected invisible watermark is robust to evasion attacks.

It turns out that this is an old problem and there is a plethora of existing work on both the design of invisible watermarks and the attacks on them. Classical invisible watermarking schemes include manipulating the least significant bit of each pixel [3] or injecting small signals in the frequency domain [18, 19].

Existing attacks on these watermarks can be categorized into two types. The first type of attack is *destructive*, where the watermark is considered part of the image and removed by corrupting the image. Typical destructive attacks include modifying the brightness or contrast of an image, JPEG compression, image rotation and adding Gaussian noise. These approaches are effective at removing watermarks but they result in significant quality loss. The second type of attack is constructive, where the watermark is treated as some noise added to the original image and removed by purifying the image. Constructive attacks include traditional image-denoising techniques like Gaussian blur [20], BM3D [21], and learning-based approaches like DnCNNs [22]. However,
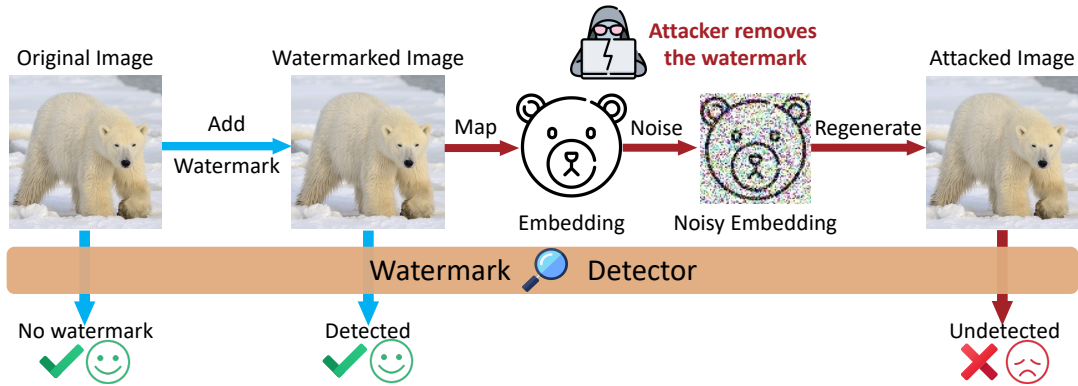
Figure 2: Removing invisible watermarks: The proposed first maps the watermarked image to its embedding, which is another representation of the image. Then the embedding is noised to destruct the watermark. After that, a regeneration algorithm reconstructs the image from the noisy embedding.

constructive attacks cannot remove resilient watermarks easily because they are not noise-like. To counter these attacks, learning-based watermarking methods [23, 24, 25] were proposed which explicitly train against these known attacks to be robust to them. But how about other attacks? What is the end of this cat-and-mouse game?

In this paper, we ask a more fundamental question:

Is an invisible watermark necessarily *non-robust?*

To be more precise, is there a fundamental tradeoff between the invisibility of a watermark and its resilience to any attack that preserves the image quality to a certain-level.

To address this question, we propose a regeneration attack that leverages the strengths of both destructive and constructive approaches. The pipeline of the attack is given in Figure 2. Our attack first corrupts the image by adding Gaussian noise to its latent representation. Then, we reconstruct the image from the noisy embedding using a generative model. The proposed regeneration attack is flexible in that it can be instantiated with various regeneration algorithms, including traditional denoisers and deep generative models such as diffusion [26]. Ironically, the recent advances in generative models that created the desperate need for invisible watermarks are also making watermark removal easier when integrated into the proposed attack.

Surprisingly, we prove that the proposed attack guarantees the removal of *any* invisible watermark such that *no* detection algorithm could work. That is to say, for any watermarks that perturb the image within a limited range of ℓ_2-distance (which is the Euclidian distance in the pixel-space), whether they have been proposed or have not yet been invented, our attack is provably effective in removing them. We also show that the image quality of the generated image is as high as if the watermark is not added in the first place.

To validate our theory empirically, we conduct extensive experiments on five widely used invisible watermarks [23, 25, 27, 28, 29] including the ones currently used by the popular open-source image generative model Stable Diffusion. We compare our attack's performance with four baselines in terms of image quality and watermark removal.

The experiment results indicate that the proposed family of attacks works significantly better than the baselines. For a particularly resilient watermark, RivaGAN, regeneration attacks remove 93-99% of the invisible watermarks while the baseline attacks remove no more than 3%. Specifically, when the denoising algorithm is set to be Stable Diffusion, our attack performs the best. With the empirical results and the theoretical guarantee, we claim that all invisible image watermarks are vulnerable to our attack and thus should not be considered in the settings where our attack applies.

Given the vulnerability of invisible watermarks, we try to explore other possibilities for image watermarking. One particular possibility that comes to our attention is the *semantic* watermarks. That is to say, we no longer want the watermarked image to look the same as the original one. As long as the watermarked image looks similar and contains similar content, it is considered suitable for use. One instance of such semantic watermark is Tree-Ring [30], which in our experiments, does show robustness against our attack. Obviously, using semantic watermarks is not a perfect solution because the watermark becomes somewhat "visible". However, with the path of invisible watermarks provably blocked, it does shed some light on protecting the proper use of AI-generated images.

1.1. Summary of Contributions

- We propose a family of regeneration attacks for image watermark removal that can be instantiated with many existing denoising algorithms and generative models.
- We prove that the proposed attack is guaranteed to remove any pixel-based invisible watermarks against any detection algorithms and regenerate images that are close to the original unwatermarked image.
- We evaluate the proposed attack on various invisible watermarks to demonstrate their vulnerability and its effectiveness compared with strong baselines, especially when instantiated with diffusion models.
- We explore other possibilities to embed watermarks in a visible yet semantically similar way. Although relaxing

the invisibility constraint is not the perfect solution, empirical results indicate that it works better under our attack and is worth looking into as an alternative.

1.2. Organization

The rest of the paper is organized as follows. Section 2 describes the problem setup for invisible watermark removal and introduces the baseline watermarking schemes, detection algorithms and attacking methods. Section 3 presents our regeneration attack family and how it can be instantiated with different denoising algorithms and pre-trained models. Section 4 contains the theoretical guarantees on certified watermark removal and the quality of regenerated images from the proposed attack. We report and analyze empirical results from watermark removal experiments under multiple settings in Section 5. Section 6 explores other possible ways to embed watermarks in an image. Some results on Tree-Ring show that relaxing the invisibility constraint and using a visible yet semantically similar watermark proves to be more robust against our attack. Section 7 reviews the existing literature on image watermarks, image steganography and attacks against them. Section 8 concludes the paper. Section 9 includes proofs not present in the main body of the paper.

2. Background

This work focuses on the removal of invisible watermarks, as opposed to visible watermarks, for several reasons. Visible watermarks are straightforward for potential adversaries to visually identify and locate within an image. Additionally, removal techniques for visible watermarks are already extensively studied in prior work such as [33, 34, 35]. In contrast, invisible watermarks do not have explicit visual cues that reveal their presence or location. Developing removal techniques for imperceptible embedded watermarks presents unique challenges.

2.1. Problem Setup

In this section, we first define invisible watermarks and the properties of an algorithm for their detection. Then, we discuss the threat model for the removal of invisible watermarks.

Definition 2.1 (Invisible watermark). Let $x \in \mathcal{X}$ be the original image and $x_w = \mathsf{Watermark}(x, \mathsf{aux})$ be the watermarked image for a watermarking scheme that is a function of x and any auxiliary information aux, e.g., a secret key. We say that the watermark is Δ-*invisible* on a clean image x w.r.t. a "distance" function dist $: \mathcal{X} \times \mathcal{X} \to \mathbb{R}_+$ if $\mathsf{dist}(x, x_w) \leq \Delta$.

Definition 2.2 (Watermark detection). A watermark detection algorithm Detect $: \mathcal{X} \times \mathsf{aux} \to \{0, 1\}$ determines whether an image $\tilde{x} \in \mathcal{X}$ is watermarked with the auxiliary information (secret key) being aux. Detect may make two types of mistakes, false positives (classifying an unwatermarked image as watermarked) and false negatives (classifying a

watermarked image as unwatermarked). $\tilde{x}$ could be drawn from either the null distribution P_0 or watermarked distribution P_1. We define Type I error (or false positive rate) $\epsilon_1 := \mathrm{Pr}_{x \sim P_0}[\mathsf{Detect}(x) = 1]$ and Type II error (or false negative rate) $\epsilon_2 := \mathrm{Pr}_{x \sim P_1}[\mathsf{Detect}(x) = 0]$.

A watermarking scheme is typically designed such that P_1 is different from P_0 so the corresponding (carefully designed) detection algorithm can distinguish them almost perfectly, that is, to ensure ϵ_1 and ϵ_2 are nearly 0.

An attack on a watermarking scheme aims at post-processing a possibly watermarked image which changes both P_0 and P_1 with the hope of increasing Type I and Type II error at the same time, hence evading the detection.

We consider the following threat model for removing invisible watermarks from images:

Adversary's capabilities. We assume that an adversary only has access to the watermarked images. The watermarking scheme Watermark, the auxiliary information aux, and the detection algorithm Detect are unknown to the adversary. The adversary can make modifications to these already watermarked images it has access to using arbitrary side information and computational resources, but it cannot rely on any specific property of the watermarking process and it cannot query Detect.

Adversary's objective. The primary objective of an adversary is to render the watermark detection algorithm ineffective. Specifically, the adversary aims to produce an image $\tilde{x}$ from the watermarked image x_w which causes the Detect algorithm to always have a high Type I error (false positive rate) or a high Type II error (false negative rate). Simultaneously, the output image $\tilde{x}$ should maintain comparable quality to the original, non-watermarked image. The adversary's objective will be formally defined later.

2.2. Invisible Watermarking Methods

In this section, we review several well-established invisible watermarking schemes that are evaluated in our experiments (Section 5). These approaches cover a range of methods, including traditional signal processing techniques and more recent deep learning methods. They include the default watermarking schemes employed by the widely used Stable Diffusion models [11]. We show some invisible watermarking examples in Figure 3

DwtDctSvd watermarking. The DwtDctSvd watermarking method [27] combines Discrete Wavelet Transform (DWT), Discrete Cosine Transform (DCT), and Singular Value Decomposition (SVD) to embed watermarks in color images. First, the RGB color space of the cover image is converted to YUV. DWT is then applied to the Y channel, and DCT divides it into blocks. SVD is performed on each block. Finally, the watermark is embedded into the blocks. DwtDctSvd is the default watermark used by Stable Diffusion.

RivaGAN watermarking. RivaGAN [23] presents a robust image watermarking method using GANs. It employs two adversarial networks to assess watermarked image

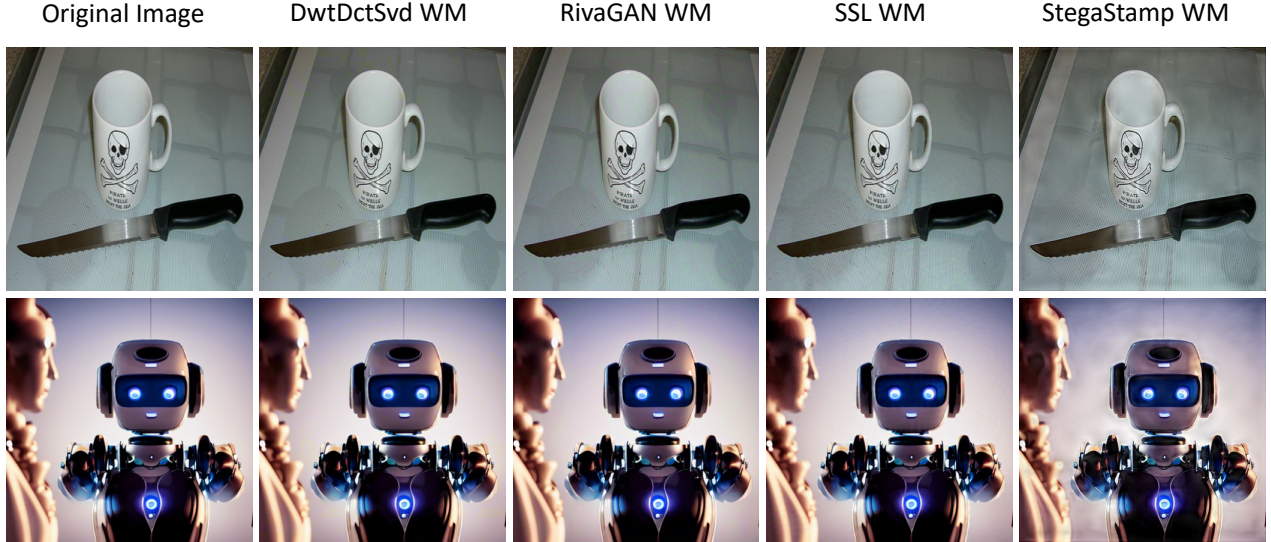| Original Image | DwtDctSvd WM | RivaGAN WM | SSL WM | StegaStamp WM |

Figure 3: Examples of different invisible watermarking methods. The top row shows real photos from the MS-COCO [31] dataset. The second row shows AI-generated content from DiffusionDB [32]. Invisible watermarks can protect both real and synthetic imagery. Of the four watermarks shown, StegaStamp introduces the most distortion and lowest quality.

quality and remove watermarks. An encoder embeds the watermark, while a decoder extracts it. By combining these, RivaGAN offers superior performance and robustness. RivaGAN is another watermark used by Stable Diffusion.

StegaStamp watermarking. StegaStamp [28] is a robust CNN-based watermarking method. It uses differentiable image perturbations during training to improve noise resistance. Additionally, it incorporates a spatial transformer network to resist minor perspective and geometric changes like cropping. This adversarial training and spatial transformer enable StegaStamp to withstand various attacks.

SSL watermarking. SSL watermarking [25] utilizes pretrained neural networks' latent spaces to encode watermarks. Networks pretrained with self-supervised learning (SSL) extract effective features for watermarking. The method embeds watermarks through backpropagation and data augmentation, then detects and decodes them from the watermarked image or its features.

Stable Signature watermarking. Stable Signature [29] fine-tunes the decoder of Latent Diffusion Models (LDM), such that the generated images have hidden invisible watermarks. The method first trains two CNN models that encode and extract watermarks in the same way as HiDDeN [36], and only keeps the watermark extractor. Then, it fine-tunes the LDM decoder to conceal a fixed watermark signature by minimizing the distance between the signature extracted by the watermark extractor and the target signature, while trying to keep the generated images close to the original one. Unlike other methods, Stable Signature merges watermarking into the generation process itself rather than using post-processing.

2.3. Invisible Watermark Detection

Watermarking methods embed k-bits of secret information into watermarked images. The watermark detection algorithm Detect, has an extractor that can then extract the hidden signal (secret bits) from watermarked images. It uses a statistical test to set a threshold for the extracted bits to decide if the extracted message closely matches the secret information.

The statistical test compares the extracted message m' to the original secret message $m \in \{0, 1\}^k$. Following previous work [37, 38] the test counts the number of matching bits $M(m, m')$. If $M(m, m') \geq \tau$ for some threshold $\tau \in \{0, \ldots, k\}$, then the image is flagged as watermarked. This allows some resilience to imperfect watermark extraction.

Formally, we test the hypothesis H_1: the image x was created by Watermark, against the null hypothesis H_0: the image was not produced by Watermark. Under H_0 (i.e., for standard images), we assume the extracted bits $m'_1, \ldots, m'_k$ are independent and identically distributed Bernoulli random variables with probability 0.5. Thus, $M(m, m')$ follows a binomial distribution $B(k, 0.5)$. The Type I error (false positive rate, ϵ_1) equals the probability that $M(m, m')$ exceeds τ, derived from the binomial cumulative distribution function. This has a closed form using the regularized incomplete beta function $I_x(a; b)$:

$$\epsilon_1(\tau) = \mathbb{P}\left(M\left(m, m'\right) > \tau \mid H_0\right) = \frac{1}{2^k} \sum_{i=\tau+1}^{k} \binom{k}{i}$$

$$= I_{1/2}(\tau + 1, k - \tau). \tag{1}$$

Decision threshold. We consider a watermark to be removed, if we can reject the null hypothesis H_0 with a p-value less than 0.01. The null hypothesis states that τ matching bits were extracted from the standard images by random chance. In practice, for a $k = 32$-bit watermark, we require at least 24 bits to be extracted correctly in order to confirm the presence of a watermark. This provides a reasonable balance between detecting real watermarks and avoiding false positives.

2.4. Existing Attacking Methods

In this section, we review common attacking methods that aim to degrade or remove invisible watermarks in images. These methods are widely used to measure the robustness of watermarking algorithms against removal or tampering [23, 25, 28, 29, 30]. The attacking methods can be categorized into destructive attacks, where the watermark is considered part of the image and actively removed by corrupting the image, and constructive attacks, where image processing techniques like denoising are used to obscure the watermark.

Destructive attacks intentionally corrupt the image to degrade or remove the embedded watermark. Common destructive attack techniques include:

Brightness/Contrast adjustment. This attack adjusts the brightness and contrast parameters of the image globally. Adjusting the brightness/contrast makes the watermark harder to detect.

JPEG compression. JPEG is a common lossy image compression technique. It has a quality factor parameter that controls the amount of compression. A lower quality factor leads to more loss of fine details and a higher chance of degrading the watermark.

Image rotation. Rotating the watermarked image by a specific angle can cause the watermark detector to fail to find the watermark. Rotation causes the synchronization between the watermark embedder and detector to be lost.

Gaussian noise. This attack adds random Gaussian noise to each pixel of the watermarked image. The variance of the Gaussian noise distribution controls the strength of the noise. A higher variance leads to more degradation of the watermark signal.

Constructive attacks aim to remove the watermark by improving image quality and restoring the original unwatermarked image. Examples include:

Gaussian blur. Blurring the image by convolving it with a Gaussian kernel smoothens the watermark signal and makes it less detectable. The kernel size and standard deviation parameter control the level of blurring.

BM3D denoising. BM3D is a highly effective image denoising technique based on Block-matching and 3D filtering [21]. It exploits self-similarities within the image to remove noise and disturbances. BM3D can attenuate watermark signals during the denoising process.

3. The Proposed Regeneration Attack

We first present in Section 3.1 an overview of the proposed regeneration attack that combines both destructive and constructive attacks. Then we demonstrate in Sections 3.2, 3.3, 3.4 how different combinations of destruction and construction algorithms can instantiate the attack. Note that information in Section 3.1 is enough for readers to get the gist of the algorithm and to understand the theoretical and empirical results. The details about specific instantiations in Sections 3.2, 3.3, 3.4 are provided for implementation references and not necessary for understanding the attack. Examples of watermark attacks are shown in Figure 3.

3.1. Overview

Our attack method first destructs a watermarked image by adding noise to its representation, and then reconstructs it from the noised representation.

Specifically, we consider the following type of algorithms specified by an embedding function $\phi : \mathbb{R}^n \to \mathbb{R}^d$, a regeneration function $\mathcal{A} : \mathbb{R}^d \to \mathbb{R}^n$ and a source of i.i.d. standard Gaussian random variables. The attack algorithm takes the watermarked image $x_w \in \mathbb{R}^n$ as input and returns

$$\hat{x} = \underbrace{\mathcal{A}\Big(\overbrace{\phi(x_w) + \mathcal{N}(0, \sigma^2 I_d)}^{\text{destructive}} \Big)}_{\text{constructive}}. \tag{2}$$

The first step of the algorithm is destructive. It maps the watermarked image x_w to an embedding $\phi(x_w)$ (which is a possibly different representation of the image), and adds some random Gaussian noise. The explicit noise shows the destructive nature of the first step. The second step of the algorithm is constructive. The corrupted image representation $\phi(x_w) + \mathcal{N}(0, \sigma^2 I_d)$ is passed through a regeneration function $\mathcal{A}$ to reconstruct the original clean image.

There are various different choices for ϕ and $\mathcal{A}$ that can instantiate our attack. ϕ can be as simple as identity map, or as complicated as deep generative models including variational autoencoders [39]. $\mathcal{A}$ can be traditional denoising algorithms from image processing and recent AI models such as diffusion [26]. The choice of ϕ and $\mathcal{A}$ may change the empirical results, but it does not affect the theoretical guarantee. In the following sections, we introduce three combinations of ϕ and $\mathcal{A}$ to instantiate the attack. Among the three, the diffusion instantiation is the most complicated and we describe it with pseudocode in Algorithm 1.

3.2. Attack Instance 1: Identity Embedding with Denoising Reconstruction

Set ϕ to be identity map, then $\mathcal{A}$ can be any image denoising algorithm, e.g., BM3D [21], TV-denoising [40], bilateral filtering [41] DnCNNs [22], or a learned natural image manifold [21, 22, 42, 43]. A particular example of interest is a "denoising autoencoder" [44], which takes ϕ to be identity, adds noise to the image deliberately, and then

Algorithm 1 Regeneration Attack Instance:
Removing invisible watermarks with a diffusion model

---

input The watermarked image x_w, a time step t^* determining the level of noise added.

output A reconstructed clean image $\hat{x}$.

1: $z_0 \leftarrow \phi(x_w)$ // map the watermarked image x_w to the latent space
2: $\epsilon \sim \mathcal{N}(0, I_d)$ // sample a random normal Gaussian noise
3: $z_{t^*} \leftarrow \sqrt{\alpha(t^*)}z_0 + \sqrt{1 - \alpha(t^*)}\epsilon$ // add noise to the latent, noise level determined by time step $t*$
4: $\hat{z}_0 \leftarrow \mathsf{solve}(z_{t^*}, t^*, s, f, g)$ // denoise the noised latent to reconstruct a clean latent
5: $\hat{x} \leftarrow \theta(z_0)$ // map the reconstructed latent back to a watermark-free image
6: **return** $\hat{x}$

---

denoises by attempting to reconstruct the image. Observe that for "denoising autoencoder" we do not need to add additional noise.

3.3. Attack Instance 2: VAE Embedding and Reconstruction

The regeneration attack in Equation 2 can be instantiated with a variational autoencoder (VAE). A VAE [39] consists of an encoder $q_\phi(z|x)$ that maps a sample x to the latent space z and a decoder $p_\theta(x|z)$ that maps a latent z back to the data space x. Both the encoder and decoder are parameterized with neural networks. VAEs are trained with a reconstruction loss that measures the distance from the reconstructed sample to the original sample and a prior matching loss that restricts the latent to follow a pre-defined prior distribution.

Instead of mapping x directly to z, the encoder maps it to the mean $\mu(x)$ and variance $\sigma(x)$ of a Gaussian distribution and samples from it. Therefore, VAE already adds noise during the encoding stage (though its variance depends on the sample x, which is not exactly the same as defined in Equation 2), so there is no need to add extra noise. Note that this is similar to the situation of denoising autoencoders described in Section 3.2, as the denoising autoencoder is a trivial case of VAE where $\mu(x)$ is identity.

3.4. Attack Instance 3: Diffusion Embedding and Reconstruction

The regeneration attack can also be instantiated with diffusion models. Diffusion models [26] define a generative process that learns to sample from an unknown true distribution $p(z_0)$. This process is learned by trying to estimate original samples from samples perturbed with random noise. In other words, diffusion models are trained to denoise, which makes them candidates for the regeneration function $\mathcal{A}$ in the proposed attack. Image-generating diffusion models either directly denoise images in the pixel space [26], or map images to latent representations and denoise in the latent space [11]. The former takes ϕ to be identity, while the latter, known as latent diffusions, takes ϕ to be the mapping function from the pixel space to the latent space. In our paper, we use latent diffusions because they are known to generate better-quality images.

For diffusion models, the process of adding noise to a clean sample is known as the *forward process*. Likewise, the process of denoising a noisy sample is known as the *backward process*. The forward process is defined by the following stochastic differential equation (SDE):

$$dz = f(z, t)dt + g(t)dw, \tag{3}$$

where $t \in [0, 1]$, $z \in \mathbb{R}^d$, $w(t) \in \mathbb{R}^d$ is a standard Wiener process, and f, g are real-valued functions. The backward process can then be described with its reverse SDE:

$$d\hat{z} = \left[f(\hat{z}, t) - g(t)^2 \nabla_{\hat{z}} \log p_t(\hat{z})\right] dt + g(t)d\bar{w}, \tag{4}$$

where $\hat{w}$ is a reverse Wiener process. Diffusion models parameterize $\nabla_{\hat{z}} \log p_t(\hat{z})$ with a neural network $s(z, t)$ and train it by minimizing the following loss

$$\int_0^1 \mathbb{E}_{p(z_0)p_t(z_t|x_0)} \left[\lambda(t)\| \log \nabla_{z_t} p_t(z_t|x_0) - s(z, t)\|_2^2\right], \tag{5}$$

where $\lambda(t)$ assigns different weights to different time steps. By substituting $s(z, t)$ into Equation 4, the backward SDE becomes known and solvable using numerical solvers [45, 46],

$$\hat{z}_0 = \mathsf{solve}(z_t, t, s, f, g). \tag{6}$$

Among many ways to define f and g in Equation 3, variance preserving SDE (VP-SDE) is commonly used [11, 26]. It defines the forward process with the following SDE,

$$dz = -\frac{1}{2}\beta(t)zdt + \sqrt{\beta(t)}dw, \tag{7}$$

where $t \in [0, 1]$, $z \in \mathbb{R}^d$, $w(t) \in \mathbb{R}^d$ is a standard Wiener process, and $\beta(t)$ is a pre-defined real valued function depicting the noise schedule. Under this setting, the conditional distribution of the noised sample is the following Gaussian [47],

$$p(z_t|z_0) = \mathcal{N}(\sqrt{\alpha(t)}z_0, 1 - \alpha(t)), \tag{8}$$

where $\alpha(t) = \exp(-\int_0^t \beta(s)ds)$. The variance of the original distribution $p(z_0)$ is preserved at any time step.

To remove invisible watermarks from images, we use VP diffusion models trained to denoise in the latent space [11]. Latent diffusion models do not directly operate on image pixels. Instead, they first map an image $x \in \mathcal{X}$ to a latent representation $z_0 = \phi(x)$ and then operate in the latent space $\mathcal{Z}$. After that, an image can be decoded from the latent representation, i.e., $\hat{x} = \theta(\hat{z}_0)$.

As defined in Algorithm 1, our algorithm removes the watermark from the watermarked image x_w (defined in Definition 2.1) using diffusion models. x_w is first mapped to the latent representation z_0, which is then noised to the time step t^*. A latent diffusion model is then used to reconstruct the latent $\hat{z}_0$, which is mapped back to an image $\hat{x}$.

Similar to denoising autoencoders, in either diffusion or VAEs, the noise-injection is integral to the algorithms themselves, and no additional noise-injection is needed.

4. Theoretical Analysis

We show in this section that the broad family of re-generation attacks as defined in Equation 2 enjoy provable guarantees on their ability to remove invisible watermarks while retaining the high quality of the original image.

4.1. Certified Watermark Removal

How do we quantify the ability of an attack algorithm to remove watermarks? We argue that if after the attack, no algorithm is able to distinguish whether the result is coming from a watermarked image or the corresponding original image without the watermark, then we consider the watermark certifiably removed. More formally:

Definition 4.1 (f-Certified-Watermark-Free). We say that a watermark removal attack is f-Certified-Watermark-Free (or f-CWF) against a watermark scheme for a non-increasing function $f : [0,1] \to [0,1]$, if for any detection algorithm $\mathsf{Detect} : \mathcal{X} \times \mathsf{aux} \to \{0,1\}$, the Type II error (false negative rate) ϵ_2 of Detect obeys that $\epsilon_2 \geq f(\epsilon_1)$ for all Type I error $0 \leq \epsilon_1 \leq 1$.

Let us also define a parameter to quantify the effect of the embedding function ϕ.

Definition 4.2 (Local Watermark-Specific Lipschitz property). We say that an embedding function $\phi : \mathcal{X} \to \mathbb{R}^d$ satisfies $L_{x,w}$-Local Watermark-Specific Lipschitz property if for a watermark scheme w that generates x_w with x,

$$\|\phi(x_w) - \phi(x)\| \leq L_{x,w} \|x_w - x\|.$$

The parameter $L_{x,w}$ measures how much the embedding compresses the watermark added on a particular clean image x. If ϕ is identity, then $L_{x,w} \equiv 1$. If ϕ is a projection matrix to a linear subspace then $0 \leq L_{x,w} \leq 1$ depending on the magnitude of the component of $x_w - x$ in this subspace. For a neural image embedding ϕ, the exact value of $L_{x,w}$ is unknown but given each x_w and x it can be computed efficiently.

Theorem 4.3. *For a Δ-invisible watermarking scheme with respect to ℓ_2-distance. Assume the embedding function ϕ of the diffusion model is $L_{x,w}$-Locally Lipschitz. The randomized algorithm $\mathcal{A}(\phi(\cdot) + \mathcal{N}(0, \sigma^2 I_d))$ produces a reconstructed image $\hat{x}$ which satisfies f-CWF with*

$$f(\epsilon_1) = \Phi\left(\Phi^{-1}(1 - \epsilon_1) - \frac{L_{x,w}\Delta}{\sigma}\right),$$

where Φ is the Cumulative Density Function function of the standard normal distribution.

Figure 4 illustrates what the tradeoff function looks like. The result says that after the regeneration attack, it is impossible for any detection algorithm to correctly detect the watermark with high confidence. In addition, it shows that such detection is as hard as telling the origin of a single sample Y from either of the two Gaussian distributions $\mathcal{N}(0,1)$ and $\mathcal{N}(L_{x,w}^2\Delta^2/\sigma^2, 1)$.
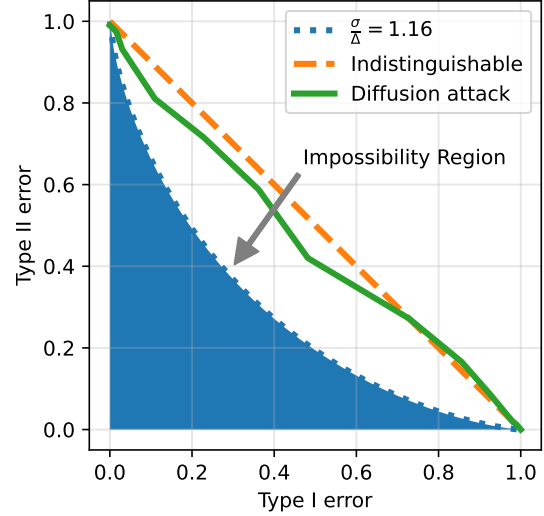

Figure 4: Theoretical and empirical trade-off functions of watermark detectors after our attack. Trade-off functions indicate how much less Type II error (false negative rate) the detector gets in return by having more Type I error (false positive rate). Theoretically, after the attack, no detection algorithm can fall in the Impossibility Region and have both Type I error and Type II error at a low level. Empirically, the watermark detector performs even worse than the theory, indicating the success of our attack and the validity of the theoretical bound. The noise level σ is set to 1.16Δ.

The proof, deferred to the end of the paper, leverages an interesting connection to a modern treatment of differential privacy [48] known as the Gaussian differential privacy [49]. The work of [49] itself is a refinement and generalization of the pioneering work of [50] and [51] which established a tradeoff-function view.

Let us instantiate the algorithm with a latent diffusion model by choosing $\sigma = \sqrt{(1 - \alpha(t^*))/\alpha(t^*)}$ (see Algorithm 1) and discuss the parameter choices.

Remark 4.4 (Two trivial cases). Observe that when $\alpha(t^*) = 0$, the result of the reconstruction does not depend on the input x_w, thus there is no information about the watermark in $\hat{x}(0)$, i.e., the trade-off function is $f(\epsilon_1) = 1 - \epsilon_2$ — perfectly watermark-free, however, the information about x (through x_w) is also lost. When $\alpha(t^*) = 1$, the attack trivially returns $\hat{x}(0) = x_w$, which does not change the performance of the original watermark detection algorithm at all (and it could be perfect, i.e., $\epsilon_1 = \epsilon_2 = 0$).

Remark 4.5 (Choice of t^*). In practice, the best choice t^* is in between the two trivial cases, i.e., one should choose it such that $L_{x,w}\Delta\sqrt{\alpha(t^*)/(1 - \alpha(t^*))}$ is a small constant. The smaller the constant, the more thoroughly the watermark is removed. The larger the constant, the higher the fidelity of the regenerated image w.r.t. x_w (thus x_0 too).

Remark 4.6 (VAE). Strictly speaking, Theorem 4.3 does

not directly apply to VAE because the noise added on the latent embedding depends on the input data. So if it chooses $\sigma(x_0) = 1$ and $\sigma(x_w) = 0$, then it is easy to distinguish between the two distributions. We can still provide provable guarantees for VAE if either the input image is artificially perturbed (so VAE becomes a denoising algorithm) or the latent space is artificially perturbed after getting the embedding vector. When $\sigma(x)$ itself could be stable, more advanced techniques from differential privacy such as Smooth Sensitivity or Propose-Test-Release can be used to provide certified removal guarantees for the VAE attack. In practice, we find that the VAE attack is very effective in removing watermarks *as is* without adding additional noise.

Remark 4.7 (The role of embedding function ϕ). Readers may wonder why having an embedding function ϕ is helpful for removing watermarks. We give three illustrative examples.

Pixel quantization. This ϕ is effective against classical Least Significant Bit (LSB) watermarks. By removing the lower-significance bits $\phi(x) = \phi(x_w)$ thus $L_{x,w} = 0$.

Low-pass filtering. By choosing ϕ to be a low-pass filter, one can effectively remove or attenuate watermarks injected in the high-frequency spectrum of the Fourier domain, hence resulting in a $L_{x,w} \ll 1$ for these watermarks.

Deep-learning-based image embedding. Modern deep-learning-based image models effectively encode a "natural image manifold," which allows a natural image x to pass through while making the added artificial watermark ϵ smaller. To be more concrete, consider ϕ to be a linear projection to a d-dimensional "natural image subspace". For a natural image x and watermarked image $x_w = x + \varepsilon$, we have $\phi(x_w) = \phi(x) + \phi(\varepsilon) = x + \phi(\varepsilon)$. If $\varepsilon \sim \mathcal{N}(0, \sigma_w^2 I_n)$ then $\mathbb{E}[\|\phi(\varepsilon)\|^2] = d\sigma_w^2 \ll n\sigma_w^2 = \mathbb{E}[\|\varepsilon\|^2]$. This projection compresses the magnitude of the watermark substantially while preserving the *signal*, thereby boosting the effect of the noise added in the embedding space in obfuscating the differences between watermarked and unwatermarked images.

Finally, we note that while Theorem 4.3 and 4.8 are specific to ℓ_2-distance, the general idea applies to other distance functions (e.g., ℓ_1 distance). ℓ_2-distance is natural for the Gaussian noise natively introduced by diffusion and VAE-based regeneration attacks.

4.2. Utility Guarantees

In this section, we prove that the regenerated image $\hat{x}$ is close to the original (unwatermarked) image x_0. This is challenging because the denoising algorithm only gets access to the noisy version of the watermarked image.

Interestingly, we can obtain a general extension lemma showing that for any black-box generative model that can successfully denoise a noisy yet unwatermarked image with high probability, the same result also applies to the watermarked counterpart, except that the failure probability is slightly larger.

Theorem 4.8. *Let x_0 be an image with n pixels and $\phi : \mathbb{R}^n \to \mathbb{R}^d$ be an embedding function. Let $\mathcal{A}$ be an image generation / denoising algorithm such that with probability at least $1 - \delta$, $\|\mathcal{A}(\phi(x_0) + \mathcal{N}(0, \sigma^2 I_d)) - x_0\| \leq \xi_{x_0, \sigma, \delta}$. Then for any Δ-invisible watermarking scheme that produces x_w from a clean image x_0, then $\hat{x} = \mathcal{A}(\phi(x_w) + \mathcal{N}(0, \sigma^2 I_d))$ satisfies that*

$$\|\hat{x} - x_0\| \leq \xi_{x_0, \sigma, \delta}$$

with a probability at least $1 - \tilde{\delta}$ where

$$\tilde{\delta} = \min_{v \in \mathbb{R}} \left\{ \delta \cdot e^v + \Phi\left(\frac{\tilde{\Delta}}{2\sigma} - \frac{v\sigma}{\tilde{\Delta}}\right) - e^v \Phi\left(-\frac{\tilde{\Delta}}{2\sigma} - \frac{v\sigma}{\tilde{\Delta}}\right) \right\}$$

in which Φ denotes the standard normal CDF and $\tilde{\Delta} := L_{x_0, w} \Delta$.

The theorem says that if a generative model is able to denoise a noisy version of the original image, then the corresponding watermark-removal attack using this generative model provably produces an image with similar quality.

Corollary 4.9. *The expression for $\tilde{\delta}$ above can be (conservatively) simplified to*

$$\tilde{\delta} \leq e^{\frac{L_{x,w}^2 \Delta^2}{2\sigma^2}} \cdot \delta^{1/2}.$$

For example if $\sigma \asymp L_{x,w} \Delta$, then this is saying that if $\xi_{x_0, \sigma, \delta}$ depends logarithmically on $1/\delta$, the same exponential tail holds for denoising the watermarked image.

The above result is powerful in that it makes no assumption about what perturbation the watermarking schemes could inject and which image generation algorithm we use. We give a few examples below.

For denoising algorithms with theoretical guarantees, e.g., TV-denoising [52, Theorem 2], our results imply provable guarantees on the utility for the watermark removal attack of the form, "w.h.p., $\frac{1}{n}\|\hat{x} - x_0\|^2 = \tilde{O}\left(\frac{\sigma \mathrm{TV}_{2d}(x_0)}{n}\right)$", i.e., vanishing mean square error (MSE) as n gets bigger.

For modern deep learning-based image denoising and generation algorithms where worst-case guarantees are usually intractable, Theorem 4.8 is still applicable for each image separately. That is to say, as long as their empirical denoising quality is good on an unwatermarked image, the quality should also be good on its watermarked counterpart.

5. Evaluation

5.1. Setup

Datasets. We evaluate our attack on two types of images - real photos taken by humans and images generated by AI systems. For real photos, we randomly sample 500 images from the MS-COCO dataset [31], a large-scale image dataset containing over 328K captioned images. For AI-generated content, we randomly sample 500 images from DiffusionDB

	MS-COCO Dataset					DiffusionDB Dataset				
Attacker	PSNR↑	SSIM↑	FID↓	Bit Acc↓	Detect Acc↓	PSNR↑	SSIM↑	FID↓	Bit Acc↓	Detect Acc↓
DctDwtSvd watermarking:										
Brightness 0.5	27.55	0.795	15.48	0.474	0.132	27.71	0.803	19.62	0.462	0.124
Contrast 0.5	26.44	0.780	12.70	0.473	0.130	26.58	0.787	17.00	0.463	0.118
JPEG 50	28.22	0.796	26.16	0.691	0.398	28.40	0.806	31.91	0.720	0.488
Rotate 90	25.41	0.756	128.45	0.356	0.000	25.51	0.763	115.26	0.366	0.000
Gaussian noise	25.02	0.736	37.94	0.996	0.996	25.13	0.744	45.78	0.989	0.988
Gaussian blur	24.99	0.742	34.09	0.999	1.000	25.10	0.750	36.60	0.999	1.000
BM3D denoise	27.66	0.783	62.59	0.577	0.090	27.94	0.795	52.21	0.623	0.190
VAE-Bmshj2018	26.95	0.767	53.64	0.528	0.006	27.25	0.780	45.74	0.538	0.006
VAE-Cheng2020	26.00	0.744	48.91	0.523	0.016	26.33	0.760	42.45	0.538	0.026
Diffusion model	25.92	0.746	46.34	0.547	0.016	26.32	0.762	48.44	0.563	0.094
RivaGAN watermarking:										
Brightness 0.5	27.59	0.793	21.60	0.990	0.998	27.75	0.803	24.26	0.934	0.906
Contrast 0.5	26.48	0.779	17.95	0.993	0.998	26.61	0.788	20.79	0.934	0.904
JPEG 50	28.26	0.795	26.98	0.953	0.982	28.44	0.806	33.45	0.880	0.816
Rotate 90	25.44	0.755	129.77	0.470	0.000	25.54	0.764	116.90	0.478	0.000
Gaussian noise	25.05	0.735	38.27	0.998	1.000	25.16	0.744	45.91	0.958	0.960
Gaussian blur	25.02	0.740	38.88	0.999	1.000	25.13	0.750	39.90	0.974	0.984
BM3D denoise	27.69	0.781	63.04	0.948	0.978	27.98	0.795	53.10	0.874	0.800
VAE-Bmshj2018	26.98	0.766	53.91	0.637	0.062	27.27	0.780	45.87	0.609	0.040
VAE-Cheng2020	26.02	0.742	48.37	0.639	0.058	26.34	0.759	41.95	0.605	0.036
Diffusion model	25.93	0.743	47.60	0.590	0.018	26.33	0.762	48.61	0.567	0.010
SSL watermarking:										
Brightness 0.5	27.61	0.792	23.92	0.999	1.000	27.82	0.801	29.24	0.991	0.996
Contrast 0.5	26.49	0.778	21.73	1.000	1.000	26.68	0.786	27.19	0.990	0.994
JPEG 50	28.27	0.793	33.06	0.808	0.800	28.52	0.804	37.65	0.759	0.616
Rotate 90	25.45	0.754	135.86	0.983	1.000	25.61	0.763	121.08	0.964	0.986
Gaussian noise	25.07	0.734	41.60	0.790	0.722	25.23	0.744	48.21	0.736	0.530
Gaussian blur	25.03	0.739	42.23	1.000	1.000	25.20	0.750	46.63	0.996	0.996
BM3D denoise	27.70	0.780	64.89	0.663	0.226	28.05	0.793	53.75	0.639	0.192
VAE-Bmshj2018	26.96	0.764	56.44	0.633	0.142	27.31	0.778	47.16	0.606	0.094
VAE-Cheng2020	25.98	0.740	50.66	0.637	0.154	26.34	0.757	43.40	0.608	0.124
Diffusion model	25.88	0.741	53.84	0.643	0.152	26.33	0.759	55.88	0.587	0.052
StegaStamp watermarking:										
Brightness 0.5	24.66	0.737	36.71	1.000	1.000	24.56	0.737	43.12	1.000	1.000
Contrast 0.5	23.76	0.729	36.20	1.000	1.000	23.66	0.728	42.38	0.999	1.000
JPEG 50	25.20	0.735	52.93	1.000	1.000	25.10	0.736	59.80	1.000	1.000
Rotate 90	22.92	0.708	142.35	0.507	0.002	22.81	0.708	124.72	0.511	0.006
Gaussian noise	22.65	0.691	56.11	1.000	1.000	22.55	0.692	63.65	1.000	1.000
Gaussian blur	22.60	0.696	51.12	1.000	1.000	22.50	0.697	57.04	1.000	1.000
BM3D denoise	24.96	0.722	82.71	1.000	1.000	24.91	0.725	73.37	1.000	1.000
VAE-Bmshj2018	24.51	0.703	68.47	0.999	1.000	24.49	0.707	64.63	1.000	1.000
VAE-Cheng2020	23.81	0.672	62.73	1.000	1.000	23.82	0.679	60.65	1.000	1.000
Diffusion model	23.67	0.665	66.84	0.863	0.992	23.76	0.673	66.63	0.859	0.990
Stable Signature watermarking:										
Brightness 0.5	28.53	0.864	11.75	0.967	0.990	28.14	0.860	16.38	0.951	0.996
Contrast 0.5	27.20	0.842	10.73	0.965	0.990	26.85	0.838	14.86	0.948	0.996
JPEG 50	29.37	0.873	15.01	0.866	0.966	28.96	0.869	19.66	0.839	0.938
Rotate 90	25.99	0.815	126.68	0.446	0.000	25.65	0.811	120.72	0.452	0.000
Gaussian noise	25.46	0.788	30.60	0.920	0.972	25.15	0.785	43.26	0.906	0.952
Gaussian blur	25.48	0.798	17.72	0.896	0.986	25.16	0.795	23.19	0.867	0.952
BM3D denoise	29.24	0.871	31.65	0.946	0.952	28.83	0.867	33.90	0.935	0.938
VAE-Bmshj2018	28.95	0.867	31.86	0.636	0.248	28.54	0.863	36.22	0.628	0.202
VAE-Cheng2020	28.67	0.864	29.43	0.682	0.442	28.28	0.861	33.89	0.655	0.334
Diffusion model	29.33	0.879	20.64	0.486	0.000	28.96	0.876	27.22	0.497	0.002

TABLE 1: Performance of attacks on different watermarking methods. The table shows attack results on MS-COCO and DiffusionDB datasets. Image quality of attacked watermarked images is compared to clean images using PSNR, SSIM, and FID. Watermark removal effectiveness is measured by average bit accuracy and detection accuracy under $p < 0.01$. Regeneration attacks (with gray background), especially the diffusion model, consistently achieve high watermark removal rates across schemes.

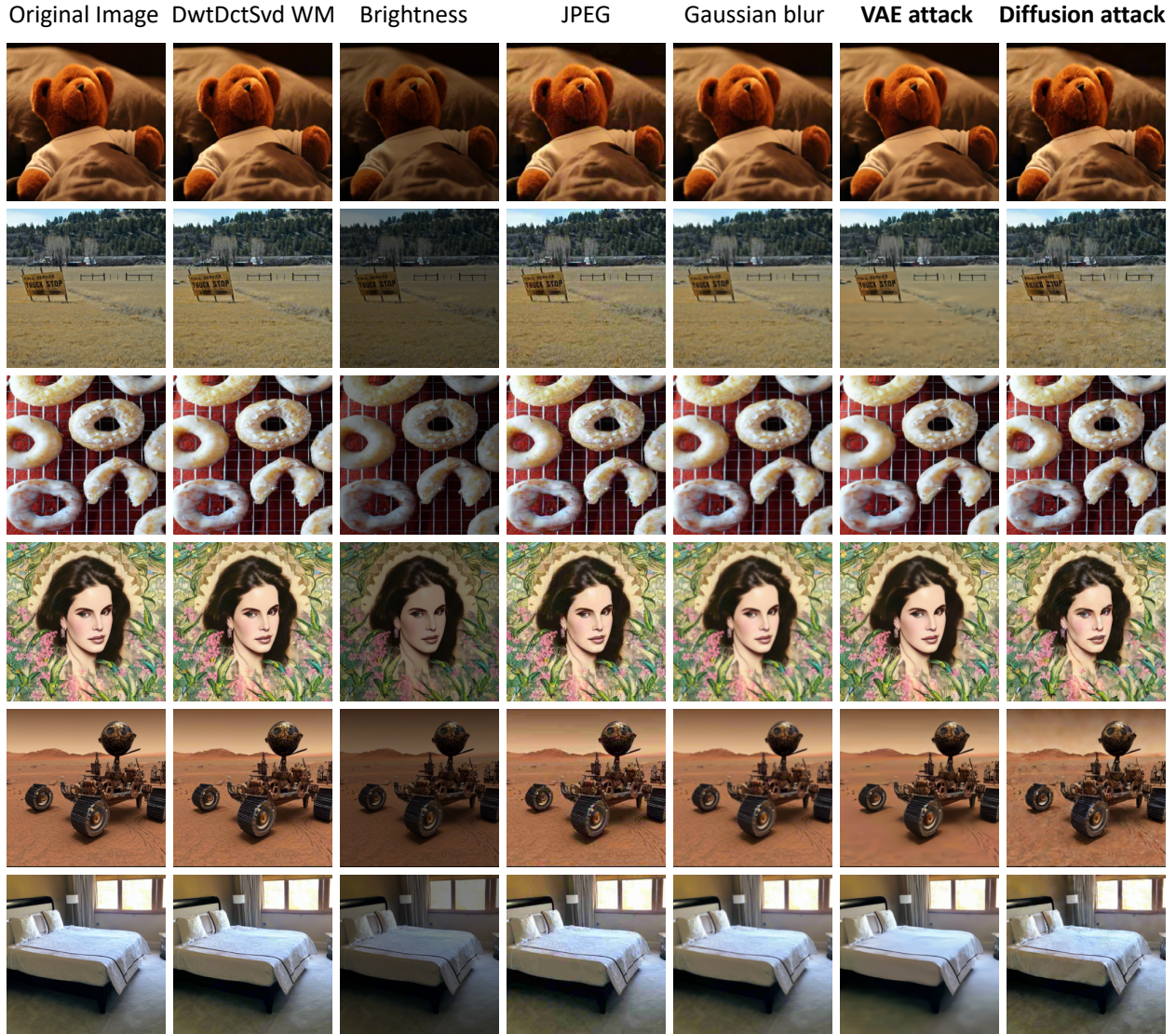| Original Image | DwtDctSvd WM | Brightness | JPEG | Gaussian blur | **VAE attack** | **Diffusion attack** |

Figure 5: Examples of watermarking attacks against DwtDctSvd, including destructive attacks like brightness change and JPEG compression, constructive attacks like Gaussian blur, and regeneration attacks using VAEs and diffusion models. Brightness change, JPEG compression, VAE attack, and diffusion attack successfully remove the watermark. The diffusion attack maintains high image quality while removing the watermark. The VAE attack over-smooths the image, resulting in blurriness.

[32], which contains 14 million images produced by Stable Diffusion using prompts and hyperparameters from real users. DiffusionDB includes both photorealistic and stylistic images such as paintings. Using these diverse datasets allows us to comprehensively test our attack on invisible watermarks across human and AI-created images.

Watermark settings. To evaluate our attack, we test five publicly available watermarking methods: DwtDctSvd [27], RivaGAN [23], StegaStamp [28], SSL watermark [25], and Stable Signature [29]. These methods represent a range of approaches, from traditional signal processing to recent deep learning techniques, as introduced in Section 2. To consider

watermarks with different lengths, we use $k = 32$ bits for DwtDctSvd, RivaGAN, and SSL watermark; $k = 96$ bits for StegaStamp; and $k = 48$ bits for Stable Signature. To detect the watermarks, we set the decision threshold to reject the null hypothesis with $p < 0.01$, requiring detection of 24/32, 61/96, and 34/48 bits corrected for the respective methods, as described in Section 2.3. For watermark extraction, we use the publicly available code for each method with default inference and fine-tuning parameters specified in their papers.

Attack baselines. To thoroughly evaluate the robustness of our proposed watermarking method, we test it against a

Watermark	COCO Dataset					Generated Dataset				
	PSNR↑	SSIM↑	FID↓	Bit Acc↑	Detect Acc↑	PSNR↑	SSIM↑	FID↓	Bit Acc↑	Detect Acc↑
DwtDctSvd	39.38	0.983	5.28	1.000	1.000	37.73	0.972	9.62	1.000	1.000
RivaGAN	40.55	0.978	10.83	1.000	1.000	40.64	0.979	13.56	1.000	1.000
SSL	41.79	0.984	18.86	1.000	1.000	41.88	0.983	23.87	0.998	1.000
StegaStamp	28.50	0.911	35.91	1.000	1.000	28.28	0.900	41.63	1.000	1.000
Stable Signature	30.87	0.898	6.28	0.990	1.000	30.75	0.900	8.29	0.980	1.000

TABLE 2: Performance of different watermarking methods. All methods successfully detect the embedded watermark.

comprehensive set of baseline attacks that represent common image perturbations. Aligning with the existing benchmark attacks summarized in Section 2.4, we select both geometric/quality distortions and noise manipulations that could potentially interfere with embedded watermarks. Specifically, the baseline attack set consists of: brightness change of 0.5, contrast change of 0.5, JPEG compression with quality 50, rotation by 90 degrees, addition of Gaussian noise with standard deviation 0.05, Gaussian blur with kernel size 5 and standard deviation 1, and the BM3D denoising algorithm with standard deviation 0.1. These manipulations represent common image processing operations that could potentially interfere with watermarks.

Proposed attacks. For attacks using variational autoencoders, we evaluate two pre-trained image compression models from the CompressAI library [53]: Bmshj2018 [54] and Cheng2020 [55]. The compression factors are set to 3 for both models. For diffusion model attacks, we use the `stable-diffusion-2-1` model from Stable Diffusion [11], a state-of-the-art generative model capable of high-fidelity image generation. The number of noise steps is set to 60 and we use pseudo numerical methods for diffusion models (PNDMs) [45] to generate samples.

Evaluation metrics. We evaluate the quality of attacked and watermarked images compared to the original cover image using two common metrics: Peak Signal-to-Noise Ratio (PSNR) defined as $PSNR(x, x') = -10 \cdot \log_{10}(MSE(x, x'))$, for images $x, x' \in [0, 1]^{c \times h \times w}$, and Structural Similarity Index (SSIM) [56] which measures perceptual similarity. To evaluate the diversity and quality of generated images, we use Fréchet Inception Distance (FID) [57] between generated and real image distributions. For images watermarked with Stable Signature, we generate watermarked and unwatermarked images using MS-COCO captions data and prompts from DiffusionDB. We evaluate FID using images generated without watermarks. To assess watermark robustness, we measure the average bit accuracy (percentage of correctly decoded bits) and average detect accuracy (percentage of images where decoded bits exceed the detection threshold). The detection threshold is set to correctly decode 24/32, 61/96, and 34/48 bits for different watermarking methods, as described in watermark settings. The experiments are conducted on Nvidia A6000 GPUs.

5.2. Results and Analysis

This section presents detailed results and analysis of the regeneration attack experiments on different watermarking methods. We evaluated five image watermarking methods - DwtDctSvd, RivaGAN, SSL, StegaStamp, and Stable Signature - under various attacks and analyzed their robustness. Some attacking examples are shown in Figure 5.

Watermarking performance without attacks. Table 2 summarizes the watermarked image quality and detection rates for images watermarked by the five methods without any attacks. All methods successfully embed and recover messages in the images. DwtDctSvd, RivaGAN, SSL, and StegaStamp are post-processing techniques that add watermarks to existing images, while Stable Signature incorporates watermarking into the image generation process. Among the post-processing methods, SSL achieves the best PSNR and SSIM, indicating higher perceptual quality compared to the original images. DwtDctSvd and Stable Signature obtain the lowest FID scores, suggesting the watermarked images have fidelity comparable to clean images. In contrast, StegaStamp shows significantly degraded quality with the lowest PSNR and highest FID. As illustrated in Figure 3, StegaStamp introduced noticeable blurring artifacts.

Watermark removal effectiveness. Table 1 summarizes the results of applying different regeneration attacks to remove watermarks. The VAE and diffusion model attacks (VAE-Bmshj2018, VAE-Cheng2020, Diffusion) consistently achieved over 90% removal rates across four out of five watermarking methods, demonstrating high effectiveness. Specifically, they remove 91-99% of DwtDctSvd watermarks, 93-99% of RivaGAN watermarks, 85-97% of SSL watermarks, and 65-100% of Stable Signature watermarks. Image rotation also shows high removal rates of for DwtDctSvd, RivaGAN, StegaStamp, and Stable Signature. However, it was ineffective against SSL, removing only 0-1% of watermarks. Since image rotation is easy to detect, a preprocessing step could allow watermark detectors to correct it. Among all watermarking methods, StegaStamp exhibits the most robustness with only 1% removal by the diffusion model and negligible removal by other attacks. The poor visual quality of StegaStamp suggests a trade-off between higher watermarked image fidelity using techniques like SSL versus more robust watermark detection achieved by StegaStamp. Overall, the consistently high removal rates across various watermarking schemes demonstrate the effectiveness of
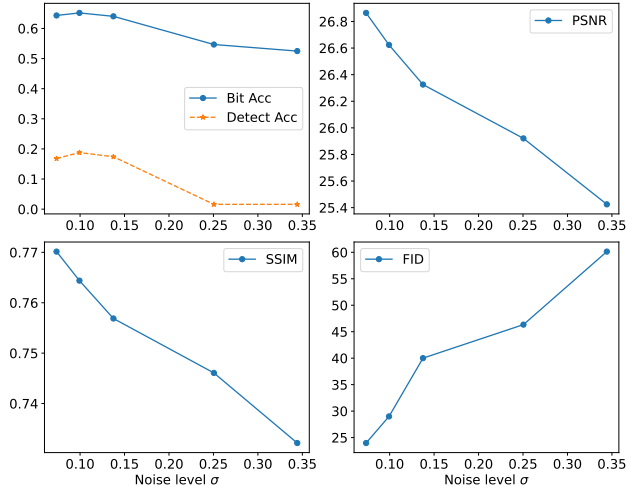
Figure 6: Regeneration attack with different diffusion steps. The noise level σ corresponds to the noising steps of $\{5, 10, 20, 60, 100\}$ for the diffusion model. Larger noise reduces watermark detection but also harms image quality, as measured by increasing PSNR and FID and decreasing SSIM. There is a trade-off between attack efficacy and image quality.

regeneration attacks for watermark removal, with diffusion models showing slightly better performance than VAEs.

Image quality reservation. The regeneration attacks generally preserved image quality well according to PSNR and SSIM. VAE models achieved higher PSNR and SSIM while diffusion models obtained better FID, indicating higher GAN-based perceptual quality. Qualitative inspection of example images in Figure 5 reveals the VAE outputs exhibit some blurring compared to the sharper diffusion outputs. Since PSNR and SSIM are known to be insensitive to blurring artifacts [58, 59], we conclude that the diffusion models better preserved image quality under attacks. All attacks resulted in negligible perceptual differences from the original images.

Watermark removal with different noise levels. To test the influence of noise level on the effectiveness of regeneration attacks, we evaluated the diffusion embedding and reconstruction attack with different denoising steps. As shown in Figure 6, we test this attack against the DwtDctSvd watermark while varying the number of denoising steps from $\{5, 10, 20, 60, 100\}$. This resulted in corresponding noise levels of σ: $\{0.07, 0.10, 0.14, 0.25, 0.34\}$. The results demonstrate that as noise level increases, watermark detection becomes more difficult. However, higher noise levels also negatively impact image quality, as evidenced by increasing PSNR and FID scores, and decreasing SSIM. This illustrates the trade-off between attack effectiveness and preservation of image quality. More aggressive noise insertion degrades watermarks more completely but also introduces more distortion.

(a) No Watermark (b) Pixel WM (c) Semantic WM

Figure 7: The image with a pixel-based watermark such as DwtDctSvd looks almost the same as the original. The image with a semantic watermark such as Tree-Ring contains the same content but is visibly different from the original. Original image generated with the prompt "an astronaut riding a horse in Zion National Park" from [30].

6. Defense with Semantic Watermarks

In this section, we discuss possible defenses that are resilient to the proposed attack, and although Theorem 4.3 has guaranteed that no detection algorithm will be able to detect the watermark after our attack, the guarantee is based on the invisibility with respect to ℓ_2 distance. Therefore, by relaxing that invisibility constraint and thus making the watermark more visible, we may be able to prevent the watermark from being removed. One less-harmful way to loosen the invisibility constraint is with semantic watermarks. As shown in Figure 7, pixel-based watermarks such as DwtDctSvd keep the image almost intact, while semantic watermarks change the image significantly but retain its content.

6.1. Tree-Ring Watermarks

Tree-Ring Watermarking [30] is a new technique that robustly fingerprints diffusion model outputs in a way that is semantically hidden in the image space. An image with a Tree-Ring watermark does not look the same as the image, but it is semantically similar (in Figure 7, both the original and the semantically watermarked image contain an astronaut riding a horse in Zion National Park). Unlike existing methods that perform post-hoc modifications to images after sampling, Tree-Ring Watermarking subtly influences the entire sampling process, resulting in a model fingerprint. The watermark embeds a pattern into the initial noise vector used for sampling. These patterns are structured in Fourier space so that they are invariant to convolutions, crops, dilations, flips, and rotations. After image generation, the watermark signal is detected by inverting the diffusion process to retrieve the noise vector, which is then checked for the embedded signal. Wen et al. [30] demonstrated that Tree-Ring Watermarking can be easily applied to arbitrary diffusion models, including text-conditioned Stable Diffusion, as a plug-in with negligible loss in FID.

6.2. Defense Experiments

To evaluate Tree-Ring as an alternative watermark, we use the same datasets from the previous experiments in

Attacker	COCO Detect Acc↓	Generated Detect Acc↓
Brightness 0.5	1.000	1.000
Contrast 0.5	1.000	1.000
JPEG 50	1.000	0.994
Rotate 90	1.000	1.000
Gaussian noise	1.000	0.996
Gaussian blur	1.000	1.000
BM3D denoise	1.000	1.000
VAE-Bmshj2018	0.998	0.994
VAE-Cheng2020	1.000	0.994
Diffusion model	1.000	0.998

TABLE 3: Tree-Ring watermarks are robust against all the tested attacks, including the ones we proposed.
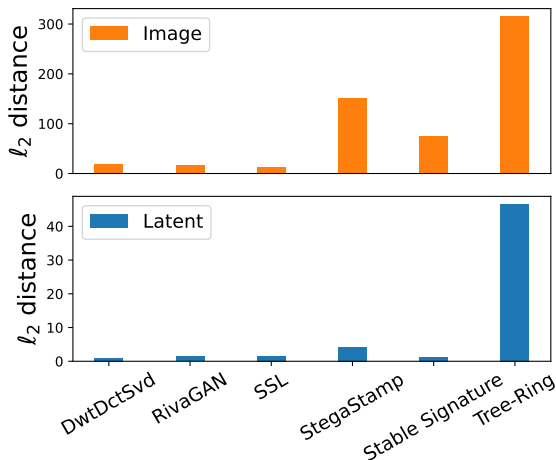

Figure 8: The ℓ_2 distances between original images and watermarked ones. Tree-Ring watermarked images are much more different in both pixel space and latent space, making Tree-Ring a *visible* watermark.

Section 5 - MS-COCO and DiffusionDB. However, since Tree-Ring adds watermarks during the generation process of diffusion, it cannot directly operate on AI-generated images. Instead, it needs textual inputs that describe the content of the images. We use captions from MS-COCO and the user prompts of DiffusionDB as the input prompts. The same set of attacks (including our proposed attack) is applied to the Tree-Ring watermarked images.

As shown in Table 3, Tree-Ring watermarks show exceptional robustness against all the attacks tested. However, such robustness does not come for free. We depict the ℓ_2-distances between original images and watermarked ones in Figure 8. Images with Tree-Ring watermarks are significantly more different from the original images in both the pixel space and the latent space. These results indicate that Tree-Ring, as an instance of semantic watermarks, shows the potential to be an alternative solution to the image watermarking problem. However, as our theory predicts, the robustness comes at the price of more visible differences.

7. Related Work

Image watermarking and steganography. Steganography and invisible watermarking are key techniques in information hiding, serving diverse purposes such as copyright protection, privacy-preserved communication, and content provenance. Early works in this area employ hand-crafted methods, such as Least Significant Bit (LSB) embedding [3], which subtly hides data in the lowest order bits of each pixel in an image. Over time, numerous techniques have been developed to imperceptibly embed secrets in the spatial [18] and frequency [19, 60] domains of an image. Additionally, the emergence of deep learning has contributed significantly to this field. Deep learning methods offer improved robustness against noise while maintaining the quality of the generated image. SteganoGAN [24] uses generative adversarial networks (GAN) for steganography and perceptual image optimization. RivaGAN [23], further improves GAN-based watermarking by leveraging attention mechanisms. SSL watermarking [25], trained with self-supervision, enhances watermark features through data augmentation. Stable Signature [29] fine-tunes the decoder of Latent Diffusion Models to add the watermark. Tree-Ring [30] proposes a semantic watermark, which watermarks generative diffusion models using minimal shifts of their output distribution.

Deep generative models. The high-dimensional nature of images poses unique challenges to generative modeling. In response to these challenges, several types of deep generative models have been developed, including Variational Auto-Encoders (VAEs) [61, 62], Generative Adversarial Networks (GANs) [63], flow-based generative models [64], and diffusion models [11, 26]. These models leverage deep latent representations to generate high-quality synthetic images and approximate the true data distribution. One particularly interesting use of generative models is for data purification, i.e., removing the adversarial noise from a data sample. The purification is similar to watermark removal except that purification is a defense strategy while watermark removal is an attack. The diffusion-based approach in [65] is similar to an instance of our regeneration attack, but the usage is different in our paper and our theoretical guarantee of watermark removal is stronger. In this paper, we aim to demonstrate the capability of these deep generative models in removing invisible watermarks from images by utilizing the latent representations obtained through the encoding and decoding processes.

8. Conclusion

We proposed a regeneration attack on invisible watermarks that combines destructive and constructive attacks. Our theoretical analysis proved that the proposed regeneration attack is able to remove any invisible watermark from images and make the watermark undetectable by any detection algorithm. We showed with extensive experiments that the proposed attack performed well empirically. The proofs and

experiments revealed the vulnerability of invisible watermarks. Given this vulnerability, we explored an alternative defense that uses visible but semantically similar watermarks. Our experiments with one instance of semantic watermark showed promising results. Our findings on the vulnerability of invisible watermarks underscore the need for shifting the research/industry emphasis from invisible watermarks to their alternatives.

References

[1] A. Z. Tirkel, G. Rankin, R. Van Schyndel, W. Ho, N. Mee, and C. F. Osborne, "Electronic watermark," *Digital Image Computing, Technology and Applications (DICTA'93)*, pp. 666–673, 1993.

[2] R. G. Van Schyndel, A. Z. Tirkel, and C. F. Osborne, "A digital watermark," in *Proceedings of 1st international conference on image processing*, vol. 2. IEEE, 1994, pp. 86–90.

[3] R. B. Wolfgang and E. J. Delp, "A watermark for digital images," in *Proceedings of 3rd IEEE International Conference on Image Processing*, vol. 3. IEEE, 1996, pp. 219–222.

[4] D. Boneh and J. Shaw, "Collusion-secure fingerprinting for digital data," *IEEE Transactions on Information Theory*, vol. 44, no. 5, pp. 1897–1905, 1998.

[5] S. A. Craver, N. D. Memon, B.-L. Yeo, and M. M. Yeung, "Can invisible watermarks resolve rightful ownerships?" in *Storage and Retrieval for Image and Video Databases V*, vol. 3022. SPIE, 1997, pp. 310–321.

[6] J. A. Bloom, I. J. Cox, T. Kalker, J.-P. Linnartz, M. L. Miller, and C. B. S. Traw, "Copy protection for dvd video," *Proceedings of the IEEE*, vol. 87, no. 7, pp. 1267–1276, 1999.

[7] M. Goljan, J. J. Fridrich, and R. Du, "Distortion-free data embedding for images," in *Information Hiding: 4th International Workshop, IH 2001 Pittsburgh, PA, USA, April 25–27, 2001 Proceedings 4*. Springer, 2001, pp. 27–41.

[8] I. J. Cox and M. L. Miller, "The first 50 years of electronic watermarking," *EURASIP Journal on Advances in Signal Processing*, vol. 2002, pp. 1–7, 2002.

[9] A. Ramesh, P. Dhariwal, A. Nichol, C. Chu, and M. Chen, "Hierarchical text-conditional image generation with clip latents," *arXiv preprint arXiv:2204.06125*, 2022.

[10] C. Saharia, W. Chan, S. Saxena, L. Li, J. Whang, E. L. Denton, K. Ghasemipour, R. Gontijo Lopes, B. Karagol Ayan, T. Salimans *et al.*, "Photorealistic text-to-image diffusion models with deep language understanding," *Advances in Neural Information Processing Systems*, vol. 35, pp. 36 479–36 494, 2022.

[11] R. Rombach, A. Blattmann, D. Lorenz, P. Esser, and B. Ommer, "High-resolution image synthesis with latent diffusion models," in *Proceedings of the IEEE/CVF Conference on Computer Vision and Pattern Recognition*, 2022, pp. 10 684–10 695.

[12] Google, "Google keynote (google i/o 23)," *Google blog*, 2023. [Online]. Available: https://io.google/2023/program/396cd2d5-9fe1-4725-a3dc-c01bb2e2f38a/

[13] K. Wiggers, "Microsoft pledges to watermark ai-generated images and videos," *TechCrunch blog*, 2023. [Online]. Available: https://techcrunch.com/2023/05/23/microsoft-pledges-to-watermark-ai-generated-images-and-videos/

[14] M. AI, "Make-a-video," *Meta website*, 2023. [Online]. Available: https://makeavideo.studio/

[15] D. Bartz and K. Hu, "Openai, google, others pledge to watermark ai content for safety, white house says," Jul 2023. [Online]. Available: https://www.reuters.com/technology/openai-google-others-pledge-watermark-ai-content-safety-white-house-2023-07-20/

[16] M. Kelly, "White house rolls out plan to promote ethical ai," May 2023. [Online]. Available: https://www.theverge.com/2023/5/4/23710533/google-microsoft-openai-white-house-ethical-ai-artificial-intelligence

[17] ——, "Chuck schumer calls on congress to pick up the pace on ai regulation," Jun 2023. [Online]. Available: https://www.theverge.com/2023/6/21/23768257/ai-schumer-safe-innovation-framework-senate-openai-altman

[18] K. Ghazanfari, S. Ghaemmaghami, and S. R. Khosravi, "Lsb++: An improvement to lsb+ steganography," in *TENCON 2011-2011 IEEE Region 10 Conference*. IEEE, 2011, pp. 364–368.

[19] V. Holub and J. Fridrich, "Designing steganographic distortion using directional filters," in *2012 IEEE International workshop on information forensics and security (WIFS)*. IEEE, 2012, pp. 234–239.

[20] O. Hosam, "Attacking image watermarking and steganography-a survey," *International Journal of Information Technology and Computer Science*, vol. 11, no. 3, pp. 23–37, 2019.

[21] K. Dabov, A. Foi, V. Katkovnik, and K. Egiazarian, "Image denoising by sparse 3-d transform-domain collaborative filtering," *IEEE Transactions on image processing*, vol. 16, no. 8, pp. 2080–2095, 2007.

[22] K. Zhang, W. Zuo, Y. Chen, D. Meng, and L. Zhang, "Beyond a gaussian denoiser: Residual learning of deep cnn for image denoising," *IEEE transactions on image processing*, vol. 26, no. 7, pp. 3142–3155, 2017.

[23] K. A. Zhang, L. Xu, A. Cuesta-Infante, and K. Veeramachaneni, "Robust invisible video watermarking with attention," *ArXiv*, vol. abs/1909.01285, 2019.

[24] K. A. Zhang, A. Cuesta-Infante, L. Xu, and K. Veeramachaneni, "Steganogan: High capacity image steganography with gans," *arXiv preprint arXiv:1901.03892*, 2019.

[25] P. Fernandez, A. Sablayrolles, T. Furon, H. J'egou, and M. Douze, "Watermarking images in self-supervised latent spaces," *ICASSP 2022 - 2022 IEEE International Conference on Acoustics, Speech and Signal Processing (ICASSP)*, pp. 3054–3058, 2021.

[26] J. Ho, A. Jain, and P. Abbeel, "Denoising diffusion probabilistic models," *Advances in Neural Information Processing Systems*, vol. 33, pp. 6840–6851, 2020.

[27] I. Cox, M. Miller, J. Bloom, J. Fridrich, and T. Kalker, *Digital watermarking and steganography*. Morgan kaufmann, 2007.

[28] M. Tancik, B. Mildenhall, and R. Ng, "Stegastamp: Invisible hyperlinks in physical photographs," in *Proceedings of the IEEE/CVF conference on computer vision and pattern recognition*, 2020, pp. 2117–2126.

[29] P. Fernandez, G. Couairon, H. Jégou, M. Douze, and T. Furon, "The stable signature: Rooting watermarks in latent diffusion models," *arXiv preprint arXiv:2303.15435*, 2023.

[30] Y. Wen, J. Kirchenbauer, J. Geiping, and T. Goldstein, "Tree-ring watermarks: Fingerprints for diffusion images that are invisible and robust," *arXiv preprint arXiv:2305.20030*, 2023.

[31] T.-Y. Lin, M. Maire, S. Belongie, J. Hays, P. Perona, D. Ramanan, P. Dollár, and C. L. Zitnick, "Microsoft coco: Common objects in context," in *Computer Vision–ECCV 2014: 13th European Conference, Zurich, Switzerland, September 6-12, 2014, Proceedings, Part V 13*. Springer, 2014, pp. 740–755.

[32] Z. J. Wang, E. Montoya, D. Munechika, H. Yang, B. Hoover, and D. H. Chau, "DiffusionDB: A large-scale prompt gallery dataset for text-to-image generative models," *arXiv:2210.14896 [cs]*, 2022. [Online]. Available: https://arxiv.org/abs/2210.14896

[33] Y. Liu, Z. Zhu, and X. Bai, "Wdnet: Watermark-decomposition network for visible watermark removal," in *Proceedings of the IEEE/CVF Winter Conference on Applications of Computer Vision*, 2021, pp. 3685–3693.

[34] A. Hertz, S. Fogel, R. Hanocka, R. Giryes, and D. Cohen-Or, "Blind visual motif removal from a single image," in *Proceedings of the IEEE/CVF Conference on Computer Vision and Pattern Recognition*, 2019, pp. 6858–6867.

[35] X. Cun and C.-M. Pun, "Split then refine: stacked attention-guided resunets for blind single image visible watermark removal," in *Proceedings of the AAAI conference on artificial intelligence*, vol. 35, no. 2, 2021, pp. 1184–1192.

[36] J. Zhu, R. Kaplan, J. Johnson, and L. Fei-Fei, "Hidden: Hiding data with deep networks," 2018.

[37] N. Yu, V. Skripniuk, S. Abdelnabi, and M. Fritz, "Artificial fingerprinting for generative models: Rooting deepfake attribution in training data," in *Proceedings of the IEEE/CVF International conference on computer vision*, 2021, pp. 14 448–14 457.

[38] N. Lukas and F. Kerschbaum, "Ptw: Pivotal tuning watermarking for pre-trained image generators," *arXiv preprint arXiv:2304.07361*, 2023.

[39] D. P. Kingma and M. Welling, "Auto-encoding variational bayes," *arXiv preprint arXiv:1312.6114*, 2013.

[40] L. I. Rudin, S. Osher, and E. Fatemi, "Nonlinear total variation based noise removal algorithms," *Physica D: nonlinear phenomena*, vol. 60, no. 1-4, pp. 259–268, 1992.

[41] C. Tomasi and R. Manduchi, "Bilateral filtering for gray and color images," in *Sixth international conference on computer vision (IEEE Cat. No. 98CH36271)*. IEEE, 1998, pp. 839–846.

[42] A. Buades, B. Coll, and J.-M. Morel, "A non-local algorithm for image denoising," in *2005 IEEE computer society conference on computer vision and pattern recognition (CVPR'05)*, vol. 2. Ieee, 2005, pp. 60–65.

[43] K. Zhang, Y. Li, W. Zuo, L. Zhang, L. Van Gool, and R. Timofte, "Plug-and-play image restoration with deep denoiser prior," *IEEE Transactions on Pattern Analysis and Machine Intelligence*, vol. 44, no. 10, pp. 6360–6376, 2021.

[44] P. Vincent, H. Larochelle, I. Lajoie, Y. Bengio, P.-A. Manzagol, and L. Bottou, "Stacked denoising autoencoders: Learning useful representations in a deep network with a local denoising criterion." *Journal of machine learning research*, vol. 11, no. 12, 2010.

[45] L. Liu, Y. Ren, Z. Lin, and Z. Zhao, "Pseudo numerical methods for diffusion models on manifolds," in *International Conference on Learning Representations*, 2021.

[46] C. Lu, Y. Zhou, F. Bao, J. Chen, C. Li, and J. Zhu, "Dpm-solver: A fast ode solver for diffusion probabilistic model sampling in around 10 steps," *Advances in Neural Information Processing Systems*, vol. 35, pp. 5775–5787, 2022.

[47] Y. Song, J. Sohl-Dickstein, D. P. Kingma, A. Kumar, S. Ermon, and B. Poole, "Score-based generative modeling through stochastic differential equations," in *International Conference on Learning Representations*, 2020.

[48] C. Dwork, F. McSherry, K. Nissim, and A. Smith, "Calibrating noise to sensitivity in private data analysis," in *Theory of Cryptography: Third Theory of Cryptography Conference, TCC 2006, New York, NY, USA, March 4-7, 2006. Proceedings 3*. Springer, 2006, pp. 265–284.

[49] J. Dong, A. Roth, and W. J. Su, "Gaussian differential privacy," *Journal of the Royal Statistical Society Series B: Statistical Methodology*, vol. 84, no. 1, pp. 3–37, 2022.

[50] L. Wasserman and S. Zhou, "A statistical framework for differential privacy," *Journal of the American Statistical Association*, vol. 105, no. 489, pp. 375–389, 2010.

[51] P. Kairouz, S. Oh, and P. Viswanath, "The composition theorem for differential privacy," in *International conference on machine learning*. PMLR, 2015, pp. 1376–1385.

[52] J.-C. Hütter and P. Rigollet, "Optimal rates for total variation denoising," in *Conference on Learning Theory*. PMLR, 2016, pp. 1115–1146.

[53] J. Bégaint, F. Racapé, S. Feltman, and A. Pushparaja, "Compressai: a pytorch library and evaluation platform for end-to-end compression research," *arXiv preprint arXiv:2011.03029*, 2020.

[54] J. Ballé, D. Minnen, S. Singh, S. J. Hwang, and N. Johnston, "Variational image compression with a scale hyperprior," *arXiv preprint arXiv:1802.01436*, 2018.

[55] Z. Cheng, H. Sun, M. Takeuchi, and J. Katto, "Learned image compression with discretized gaussian mixture likelihoods and attention modules," in *Proceedings of the IEEE/CVF Conference on Computer Vision and Pattern Recognition*, 2020, pp. 7939–7948.

[56] Z. Wang, A. C. Bovik, H. R. Sheikh, and E. P. Simoncelli, "Image quality assessment: from error visibility to structural similarity," *IEEE transactions on image processing*, vol. 13, no. 4, pp. 600–612, 2004.

[57] M. Heusel, H. Ramsauer, T. Unterthiner, B. Nessler, and S. Hochreiter, "Gans trained by a two time-scale update rule converge to a local nash equilibrium," *Advances in neural information processing systems*, vol. 30, 2017.

[58] P. Ndajah, H. Kikuchi, M. Yukawa, H. Watanabe, and S. Muramatsu, "Ssim image quality metric for denoised images," in *Proc. 3rd WSEAS Int. Conf. on Visualization, Imaging and Simulation*, 2010, pp. 53–58.

[59] Z. Wang, A. Bovik, H. Sheikh, and E. Simoncelli, "Image quality assessment: from error visibility to structural similarity," *IEEE Transactions on Image Processing*, vol. 13, no. 4, pp. 600–612, 2004.

[60] T. Pevný, T. Filler, and P. Bas, "Using high-dimensional image models to perform highly undetectable steganography," in *Information Hiding: 12th International Conference, IH 2010, Calgary, AB, Canada, June 28-30, 2010, Revised Selected Papers 12*. Springer, 2010, pp. 161–177.

[61] P. Vincent, H. Larochelle, Y. Bengio, and P.-A. Manzagol, "Extracting and composing robust features with denoising autoencoders," in *Proceedings of the 25th international conference on Machine learning*, 2008, pp. 1096–1103.

[62] A. Van Den Oord, O. Vinyals *et al.*, "Neural discrete representation learning," *Advances in neural information processing systems*, vol. 30, 2017.

[63] I. Goodfellow, J. Pouget-Abadie, M. Mirza, B. Xu, D. Warde-Farley, S. Ozair, A. Courville, and Y. Bengio, "Generative adversarial networks," *Communications of the ACM*, vol. 63, no. 11, pp. 139–144, 2020.

[64] D. Rezende and S. Mohamed, "Variational inference with normalizing flows," in *International conference on machine learning*. PMLR, 2015, pp. 1530–1538.

[65] W. Nie, B. Guo, Y. Huang, C. Xiao, A. Vahdat, and A. Anandkumar, "Diffusion models for adversarial purification," in *International Conference on Machine Learning*. PMLR, 2022, pp. 16 805–16 827.

[66] B. Balle and Y.-X. Wang, "Improving the gaussian mechanism for differential privacy: Analytical calibration and optimal denoising," in *International Conference on Machine Learning*. PMLR, 2018, pp. 394–403.

[67] I. Mironov, "Rényi differential privacy," in *IEEE computer security foundations symposium (CSF)*. IEEE, 2017, pp. 263–275.

9. Proofs of Technical Results

Proof of Theorem 4.3. By the conditions on the invisible watermark and the local Lipscthiz assumption on ϕ, we get that

$$\|\phi(x_0) - \phi(x_w)\|_2 \le L_{x_0,w}\Delta.$$

This can be viewed as the ℓ_2-local-sensitivity of ϕ at x_0 in the language of differential privacy literature.

By [49][Theorem 2.7] (Gaussian mechanism), we get that the tradeoff function is as stated.

Finally, by [49][Proposition 2.8] (postprocessing), the tradeoff function for the generated image $\hat{x}$ also satisfies the same tradeoff function as stated. □

Proof of Theorem 4.8. The key idea is to use the definition of indistinguishability (differential privacy, but for a fixed pair of neighbors, rather than for all neighbors). So we say two input x, x' are (v, w)-indistinguishable using the output of a mechanism $\mathcal{M}$ if for any event S,

$$\Pr[\mathcal{M}(x) \in S] \le e^v \Pr[\mathcal{M}(x') \in S] + w.$$

and the same also true when x, x' are swapped. In our case, we have already shown that (from the proof of Theorem 4.3) for any post-processing algorithm $\mathcal{A}$, x_0 and x_w are indistinguishable using $\hat{x}$ in the trade-off function sense. [66] obtained a "dual" characterization which says that the same Gaussian mechanism satisfies (v, w)-indistinguishability with

$$w = \Phi\left(\frac{\tilde{\Delta}}{2\sigma} - \frac{v\sigma}{\tilde{\Delta}}\right) - e^v \Phi\left(-\frac{\tilde{\Delta}}{2\sigma} - \frac{v\sigma}{\tilde{\Delta}}\right)$$

for all $v \in \mathbb{R}$. By instantiating the event S to be that $\|\hat{x} - x_0\| \le \xi_{x_0,\sigma,\delta}$, then we get

$$\Pr_{x_w}[\|\hat{x} - x_0\| \le \xi_{x_0,\sigma,\delta}] \le e^v \Pr_{x_0}[\|\hat{x} - x_0\| \le \xi_{x_0,\sigma,\delta}] + w$$
$$= e^v \cdot \delta + w.$$

This completes the proof. □

Proof of Corollary 4.9. The w, v "privacy profile" implies a Renyi-divergence bound (one can also get that directly from the Renyi-DP of gaussian mechanism) which implies (by Proposition 10 of [67]) that

$$\tilde{\delta} \le \min_{u \ge 1} \left(e^{\frac{u\tilde{\Delta}^2}{2\sigma^2}} \cdot \delta\right)^{(u-1)/u}.$$

The stated result is obtained by setting $u = 2$. □